Investigation of the RF efficiency of Inductively Coupled Hydrogen Plasmas at 1 MHz

D. Rauner[1,2,a)], S. Mattei[3,4], S. Briefi[2], U. Fantz[1,2], A. Hatayama[5], J. Lettry[3], K. Nishida[5] and M. Q. Tran[4]

[1]*Max-Planck-Institut für Plasmaphysik, Boltzmannstr. 2, 85748 Garching, Germany*
[2]*AG Experimentelle Plasmaphysik, Universität Augsburg, 86135 Augsburg, Germany*
[3]*CERN, 1211 Geneva 23, Switzerland*
[4]*Swiss Plasma Center, Ecole Polytechnique Federale de Lausanne, CH-1015 Lausanne, Switzerland*
[5]*Graduate school of Science and Technology, Keio University, 3-14-1 Hiyoshi, Kouhoku-ku, Yokohama 223-8522, Japan*

[a)]Corresponding author: david.rauner@ipp.mpg.de

Abstract. The power requirements of RF heated sources for negative hydrogen ions in fusion are substantial, which poses strong demands on the generators and components of the RF circuit. Consequently, an increase of the RF coupling efficiency would be highly beneficial. Fundamental investigations of the RF efficiency in inductively coupled hydrogen and deuterium discharges in cylindrical symmetry are conducted at the lab experiment CHARLIE. The experiment is equipped with several diagnostics including optical emission spectroscopy and a movable floating double probe to monitor the plasma parameters. The presented investigations are performed in hydrogen at a varying pressure between 0.3 and 10 Pa, utilizing a conventional helical ICP coil driven at a frequency of 1 MHz and a fixed power of 520 W for plasma generation. The coupling efficiency is strongly affected by the variation in pressure, reaching up to 85 % between 1 and 3 Pa while dropping down to only 50 % at 0.3 Pa, which is the relevant operating pressure for negative hydrogen ion sources for fusion. Due to the lower power coupling, also the measured electron density at 0.3 Pa is only $5 \cdot 10^{16}\,\mathrm{m}^{-3}$, while it reaches up to $2.5 \cdot 10^{17}\,\mathrm{m}^{-3}$ with increasing coupling efficiency. In order to gain information on the spatially resolved aspects of RF coupling and plasma heating which are not diagnostically accessible, first simulations of the discharge by an electromagnetic Particle-In-Cell Monte Carlo collision method have been conducted and are compared to the measurement data. At 1 Pa, the simulated data corresponds well to the results of both axially resolved probe measurements and radially resolved emission profiles obtained via OES. Thereby, information regarding the radial distribution of the electron density and mean energy is provided, revealing a radial distribution of the electron density which is well described by a Bessel profile.

INTRODUCTION

RF heated sources for negative hydrogen ions for the neutral beam heating of fusion experiments require very high RF powers to achieve the necessary H^- currents. For example, at the ion source of the ITER neutral beam heating system which will be equipped with 8 cylindrical discharge vessels, the so-called drivers, a maximum RF power of 100 kW per driver is planned [1, 2]. A reduction of the RF power would be highly beneficial, as such high powers pose strong demands on all components of the RF circuit and the generators. However, the plasma parameters required for a satisfactory source performance must be sustained [3]. A promising approach to achieve a reduction of the required power is the increase of the RF coupling efficiency, which is defined as the relative fraction of the totally delivered RF power which is actually absorbed by the plasma itself, as there is always a second fraction which is lost, e.g. due to the heating of the coil and induced eddy currents. The investigation of the RF coupling efficiency, or by analogy the effective plasma resistance, is commonly used for the optimization of inductively and capacitively coupled plasmas [4, 5, 6].

Therefore, fundamental investigations of the RF coupling efficiency for inductive plasma heating as well as regarding possible alternatives such as helicon coupling are performed at the lab experiment CHARLIE. Due to its

flexibility, it allows for various systematic investigations in continuous wave hydrogen and deuterium operation, including e.g. the application of different antenna types and the influence of external magnetic fields on the plasma parameters [7, 8, 9]. In addition to the 13.56 MHz / 600 W generator already available, the experiment has recently been equipped with a 1 MHz / 1 kW generator, which allows for dedicated investigations at the excitation frequency relevant for ITER. Furthermore, the diagnostic setup has been extended by a system to directly measure the RF coupling efficiency based on an approach by [4]. In combination with the further diagnostic systems including electrical probes (moveable along the cylinder axis of the vessel) and optical emission spectroscopy, this setup allows for investigations of the correlation between the RF coupling efficiency and the plasma parameters essential for negative ion sources. In this contribution, investigations performed in hydrogen at 1 MHz are presented, utilizing a conventional helical ICP coil. The measurements are performed at a fixed RF power of 520 W for pressures between 0.3 and 10 Pa. In order to gain information on the spatially resolved aspects of RF coupling and plasma heating in addition to the experimental work, first simulations of the discharge by an electromagnetic Particle-In-Cell Monte Carlo collision method have been conducted . The code, described in [10], simulates the RF-heating of the plasma based on the real experiment geometry, thereby providing spatial distributions of the plasma parameters which are not diagnostically accessible with the current setup, particularly the radial profiles of the electron density and temperature. For an operating pressure of 1 Pa, first results of a comparison of the modelled data with axial profiles of the plasma density and the electron energy obtained via probe measurements and with radial emission profiles of the atomic H_β line obtained via OES are presented.

EXPERIMENTAL SETUP AND APPLIED DIAGNOSTICS

A sketch of the CHARLIE experiment (**C**oncept studies for **H**elicon **A**ssisted **RF** **L**ow pressure **I**on sourc**E**s) is shown in Figure 1, along with the applied diagnostics. Hydrogen discharges are generated in continuous wave operation in a cylindrical quartz glass vessel of the length of 40 cm and the inner diameter of 9 cm. The vacuum system is attached at the ends of the cylinder, including a capacitance manometer. Operating pressures are in the range between 0.3 and 10 Pa in H_2, for the presented investigations the gas flow is fixed at 5 sccm. The RF circuit consists of a generator operating at 1 MHz, which provides a maximum power output of 1 kW, the corresponding matching unit and the helical coil made of copper pipe (5 windings) for inductive plasma operation which is centred with respect to the vessel axis. For all investigations presented in this contribution, the output RF power $P_{\mathrm{RF,del}} = P_{\mathrm{set}} - P_{\mathrm{refl}}$ was fixed at 520 W.

V-I-probe and current transformer

Between the generator and the matching unit a V-I probe for in-line RF voltage, current and phase angle measurement is installed. It allows for the real-time monitoring and control of the impedance matching of plasma, RF coil and matching unit to the generator source impedance of 50 Ω. Additionally, a precise quantification of the totally delivered RF power $P_{\mathrm{RF,del}}$ is possible. During all measurements presented in this contribution, impedance matching is perfectly achieved by adjusting the variable capacitors of the matching circuit. Consequently, $P_{\mathrm{RF,del}}$ corresponds to the set output power of the RF generator and the reflected power is zero within the measurement accuracy. To quantify the RF current through the plasma coil $I_{\mathrm{ant,rms}}$, a RF current transformer is installed around the connection between the matching unit and the coil. In combination with an oscilloscope, $I_{\mathrm{ant,rms}}$ is measured time resolved. The installed systems as well as the measured parameters are also depicted in Figure 1.

This combination of both the V-I-probe and the current transformer allows for the precise measurement of the power which is actually absorbed by the plasma itself. Typically, the total delivered RF power $P_{\mathrm{RF,del}}$ is split into a part P_{plasma} which actually contributes to the plasma heating, and a part P_{network} which is deposited due to ohmic heating in the matching network and the coil as well as via induced eddy currents within conductors in the vicinity of the coil, e.g. the metallic parts of the vacuum system and the vessel end plates. This fraction of the power is lost with respect to the original goal, the plasma heating. By analogy, the relative fraction of the delivered power which is coupled into the plasma is defined as the RF coupling efficiency η:

$$P_{\mathrm{RF,del}} = P_{\mathrm{plasma}} + P_{\mathrm{network}} \quad \Leftrightarrow \quad \eta = \frac{P_{\mathrm{plasma}}}{P_{\mathrm{RF,del}}} = \frac{P_{\mathrm{RF,del}} - P_{\mathrm{network}}}{P_{\mathrm{RF,del}}} \tag{1}$$

In order to quantify and evaluate the coupling efficiency and the power coupled to the plasma, a commonly used approach is to measure the power losses P_{network}. The exact procedure which was applied for the results presented

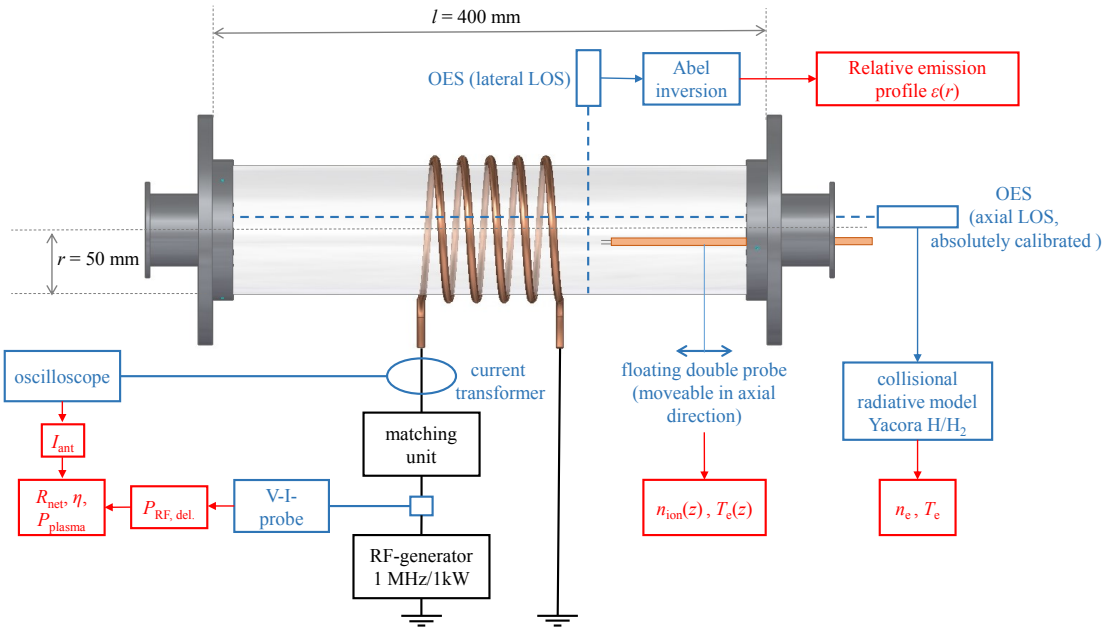

FIGURE 1. Experimental and diagnostic setup of CHARLIE.

here is described in [4]. It is based on the determination of the real part of the impedance of the matching network R_{network}, which also includes the resistance of the plasma coil: via operating the experiment in pure vacuum, plasma ignition is suppressed when the RF generator is switched on. By a variation of the delivered RF power $P_{\text{del,vac}}$ and the measurement of the current running through the plasma coil, R_{network} can then be deduced according to $P_{\text{del,vac}} = R_{\text{network}} I^2_{\text{vac,rms}}$ since no power absorption by the plasma takes place. With the knowledge of the network resistance and the coil current directly measured during plasma operation, the power dissipated in the network during plasma is then consequently given by $P_{\text{network}} = R_{\text{network}} I^2_{\text{pla,rms}}$. With this information, the power absorbed by the plasma itself – and respectively the coupling efficiency – can be calculated according to Equation (1).

Floating double probe

The investigated discharge is mainly created within the dielectric quartz vessel and has only little contact to the metallic vessel end plates. Due to this lack of a conducting wall which can be used as a reference point for electric potentials, the application of a common Langmuir probe is not feasible. Therefore, a floating double probe is used [11, 12]. As depicted in Figure 1, the probe is fed through one end plate with a distance of 1 cm to the vessel centre, and can be moved parallel to the cylinder axis within 20 cm, allowing to measure spatial profiles. The probe itself consists of two identical tungsten wires of a length of 10 mm and a diameter of 300 µm. Via the floating double probe, the ion density n_{ion} and the electron temperature T_{e} are determined [12]. For the evaluation and comparison of the measured density with further diagnostics and modelling, quasineutrality ($n_{\text{ion}} = n_{\text{e}}$) is assumed.

Optical emission spectroscopy and collisional radiative modelling

Optical emission spectroscopy is performed at two different line of sights (LOS) which are shown in Figure 1. Investigations are conducted via a high resolution spectrometer ($\Delta\lambda_{\text{FWHM}} = 18$ pm) which is intensity calibrated within the wavelength region of 250 to 800 nm. The first LOS is oriented parallel and in the distance of 1 cm to the cylinder axis and crosses the plasma over the whole length of 40 cm. The absolute emission of both the atomic Balmer series as well as the molecular Fulcher system ($d^3\Pi_u \rightarrow a^3\Sigma_g^+$), which is the most intense transition of H_2 in the optical

wavelength region, is detected along this line of sight. Among other parameters, the evaluation of the Fulcher system allows for a determination of the gas temperature T_{gas} during plasma operation [13]. The exact procedure of the evaluation which was applied to determine the gas temperature follows an improved method described in [14]. Since both the gas temperature and the pressure are known, the neutral particle density of the plasma is given by the ideal gas law. Furthermore, an evaluation of the measured emissivities of the atomic and molecular transitions by the collisional radiative model Yacora H & H_2 [15, 16] allows for the determination of the electron density n_e and the electron temperature T_e, both averaged along the LOS. The second line of sight of the OES is oriented laterally to the cylinder vessel and is mounted movable along and perpendicular to the cylinder axis. For the investigations presented here, it is used to measure intensity profiles of the atomic Balmer line H_β across the vessel diameter at a fixed axial position 70 mm distant to the vessel centre. Via Abel inversion, the lateral intensity profiles are numerically transformed into radial emission profiles $\epsilon(r)$ [17]. For this setup, the followed approach is described in detail in [7]. Requirements for an application of the Abel inversion are the cylindrical symmetry of the discharge and a negligible optical thickness of the detected emission line. Due to the geometry of the experiment and the low population density of the lower state $n = 2$ of the H_β line, both requirements are fulfilled for this setup [7].

PIC-MCC modelling

The electromagnetic Particle-In-Cell Monte Carlo collision method which was applied for the simulation of the steady state operation of the experiment is described in detail in [10]. The model takes into account the real experimental geometry and consists of a 2.5D model of the axisymmetric electromagnetic field and a 3D3V particle dynamics model of the charged particles (e^-, H^+, H_2^+, H_3^+, H^-) and the neutral species H and H_2. As the antenna is treated as a perfect inductor leading a given current, the plasma heating mechanism is purely inductive. The applied Monte Carlo collision model takes into account over 200 electron and ion collisions processes, including elastic collisions, ionization and molecular vibrational excitation of H_2. Due to the low ionization degree of the plasma ($\alpha \lesssim 0.1\%$), electron-electron collisions are neglected to save computational time. For the simulation of CHARLIE, the volume is subdivided in square cells of 5 mm side length. Beside the geometry data of the experiment, the required input parameters for the calculations are the antenna current, which is measured via the current transformer, and the neutral particle density, which can be deduced from the plasma pressure and the gas temperature.

RESULTS

Coupling efficiency and plasma parameters

In Figure 2 (a), the root mean square of the RF current through the plasma coil and the evaluated RF coupling efficiency η are shown for the fixed RF power of 520 W. The pressure is varied between 0.3 Pa and 10 Pa. The antenna current shows a broad minimum of roughly 28 A at operating pressures between 1 and 3 Pa and increases significantly for both lower and higher pressure. The maximum current of more than 50 A is obtained at the low pressure limit of 0.3 Pa. The second parameter required for the analysis of the coupling efficiency, the network resistance $R_{network}$, appears to be almost constant with varying pressure remaining at $0.09 \pm 0.01\ \Omega$ for all presented measurements. The reason of the weak variation is the relatively minor variation of the matching capacitors which was required to achieve impedance matching. Therefore, the behaviour of the RF coupling efficiency is according to Equation (1) mainly dominated by the variation of the RF current. Consequently, the pressure dependency of η is inverse to the RF current, reaching its maximum of 85 % between 1 and 3 Pa. Analogously, with increasing current at lower and higher pressure the ohmic losses increase and the coupling efficiency decreases, reaching its minimum of only 50 % at 0.3 Pa. However, this low value is only valid for this experiment at the fixed delivered power of 520 W. Further investigations which are not presented here indicate an increase of η at low pressures with increasing RF power, an observation which has also been made in other discharges [4, 5]

Generally, a comparable pressure dependant behaviour of the coupling efficiency is known from various investigations using different inert gases [4, 5, 18]. Typically, a maximum of the RF coupling efficiency and power absorption by the plasma is expected for the case when the effective electron collision frequency ν_e equals the excitation frequency ω_{RF}, which corresponds to the maximum of the real part of the RF plasma conductivity [19, 4]. If the pressure is significantly decreased ($\nu_e \ll \omega_{RF}$) or increased ($\nu_e \gg \omega_{RF}$), the plasma conductivity is lowered. Consequently, if the power absorption by the plasma is fixed, either the volume of excitation or the induction electric field has to increase [19]. This however requires an increase of the RF magnetic flux, which is consecutively achieved

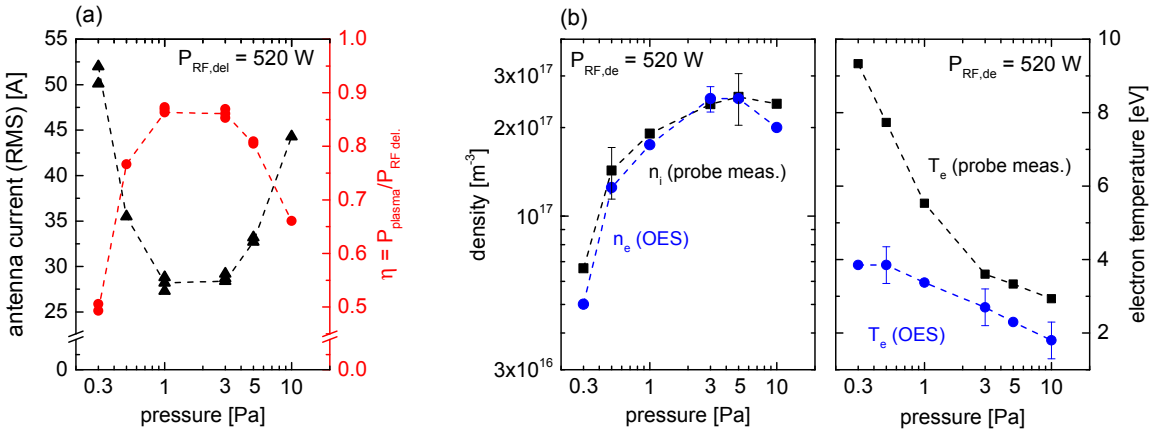

FIGURE 2. (a) Antenna current and coupling efficiency η at varying pressure. (b) Pressure dependence of the ion density and electron density on the left and the electron temperature on the right. Presented are the values obtained via the floating double probe as well as via OES and collisional radiative modelling.

by the rising antenna current. A simple estimation of the electron collision frequency ν_e based on cross section data by [20] revealed that $\nu_e \approx \omega_{RF}$ is fulfilled within the pressure range of 0.5 and 2 Pa, which indicates the validity of the pressure dependent behaviour described above also for hydrogen.

Additionally to the investigation of the coupling efficiency, the plasma parameters are measured via OES and the floating double probe. The space resolved values of n_{ion} and T_e obtained by the probe show strong axial variations with a peak in the central region below the RF coil, which are explicitly shown in the next section. For the comparison with the LOS-integrated OES data however, these profiles are averaged along the axis. The results are presented in Figure 2 (b). The evaluated axial averages of the electron density evaluated via OES and the ion density provided by the floating double probe are in excellent absolute and relative agreement over the whole pressure range and increase from $0.5 \cdot 10^{17}$ m^{-3} at 0.3 Pa to a peak value of approximately $2.5 \cdot 10^{17}$ m^{-3} between 3 and 5 Pa. The electron temperature evaluated via OES is characterized by a monotonous decrease (from 3.9 eV at 0.3 Pa to 1.8 eV at 10 Pa), which corresponds to the expected behaviour in low pressure discharges. The electron temperature evaluated via the probe measurements shows a comparable relative pressure dependence, but the absolute values are roughly a factor of 2 higher than those obtained via OES and are further increasing especially at low pressure. However, this deviation can be contributed to the fact that the floating double probe can only detect electrons within the high energetic tail of the electron energy distribution function (EEDF) [12]. Therefore, the error of this method can be significantly high, especially if the EEDF is non-Maxwellian which is typical for low-pressure discharges [21].

Comparison of modelled and measured spatial profiles

Via the additional information provided by the PIC-MCC simulations, further insight on the plasma parameters can be gained, in particular on their radial distribution which is not diagnostically accessible with the present setup. To ensure the general comparability of measurement and simulation, in a first step the axial profiles of the simulated values of the electron density n_e and mean energy E_e are compared to the axial profiles of the plasma parameters n_{ion} and $T_e = 2/3 k_B E_e$ measured by the floating double probe at the pressure of 1 Pa. This scenario is chosen due to its high coupling efficiency of 85 %, as the model is simulating pure inductive heating. If the coupling efficiency decreases, capacitive coupling might have an increasing influence which cannot be accounted for in the model. At 1 Pa the antenna current is 28.2 A and the neutral particle density, which is derived by the ideal gas law at a gas temperature of 590 K, is $1.2 \cdot 10^{19}$ m^{-3}. As initial conditions, an electron density of 10^{16} m^{-3} and an electron temperature of 1 eV is chosen. After a simulated time of roughly 10 µs, the calculated particle densities and temperatures (except for the vibrational population of H_2) reach steady state. All values presented in the following are time averaged over the last RF cycle.

The comparison of the axial profiles of the densities and the mean electron energy is shown in Figure 3. The

simulated data is radially averaged at a distance of 10 ± 5 mm to the vessel axis in order to match the position of the probe measurement. Additionally depicted via the dashed lines are axially averaged values which allow for a comparison of the absolute values obtained by OES. For the density, the measured values describe a peaked profile with its maximum of $4 \cdot 10^{17}$ m^{-3} below the coil. The simulation shows a similar behaviour of the electron density, but reaches up to $6 \cdot 10^{17}$ m^{-3} in the vessel centre. As its relative profile is furthermore slightly less broadened than the profile of the measurement, the axially averaged density values of the probe, the OES and the simulation show a very good agreement within $(2 \pm 0.2) \cdot 10^{17}$ m^{-3}. Regarding the deviations of the relative profile, two possible explanations can be given for a broadening of the measured profile with respect to the simulation. On the one hand, the invasive probe measurement can influence the plasma: when the probe is moved below the coil, the plasma generation is hindered leading to a decreased density. On the other hand, even though the inductive heating of the plasma is dominant as the coupling efficiency is high, capacitive coupling is still present to a minor extent (as it is not suppressed, e.g. by a Faraday screen). Due to the occurring RF voltages, this could lead to a slight increase of the density especially between the coil and the vessel end plates, which is not accounted for in the model.

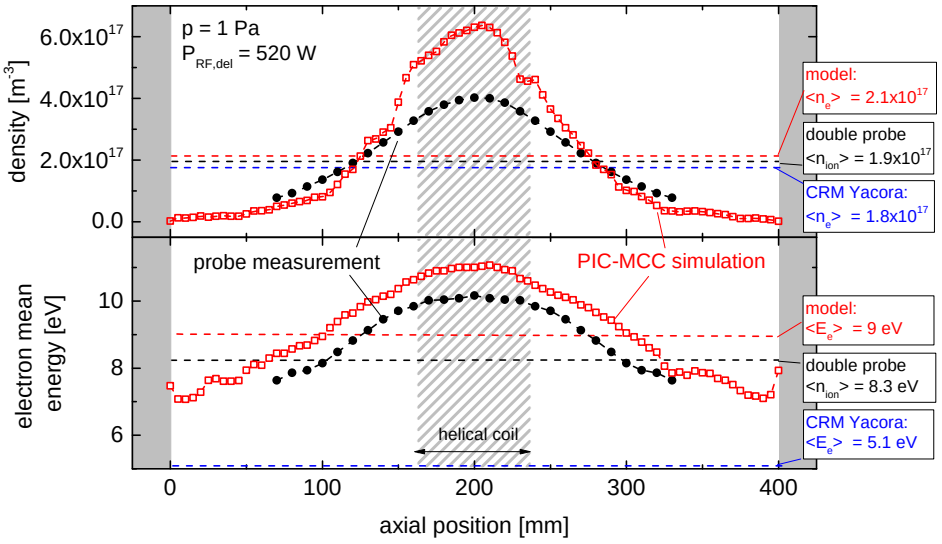

FIGURE 3. Comparison of the axial profiles of the ion density and electron energy measured via the floating double probe with the axial profiles of the electron density and energy provided by the PIC-MCC model for a pressure of 1 Pa.

The mean electron energy shows a peaked profile as well. Generally, a very good agreement between probe measurement and simulation is achieved regarding the relative behaviour. However, the absolute values obtained by the model systematically exceed the probe measurements by roughly 1 eV, reaching a maximum value of 11 eV below the coil. Particularly the deviation from the electron energy obtained by the spectroscopic investigations is significant. The origin of this difference is subject of further investigations. Possible reasons might be the contribution of the particle drift energy included in the simulated mean electron energy or the significantly non-maxwellian EEDF of the simulation (in comparison to the assumption of a purely maxwellian EEDF for the OES evaluation).

Despite the absolute deviations between the model and the measurement, a good agreement particularly with respect to the relative behaviour of both profiles is found. This allows for the assumption, that also the relative radial profiles of both the simulated plasma density and energy represent the actual radial profiles of the discharge, which are not directly accessible with the diagnostic setup. The spatial distribution of the simulated n_e and E_e over the vessel diameter is shown in Figure 4 (a). In order to reduce the fluctuation of the modelled data and account for the symmetry of the discharge, the profiles are evaluated by averaging the radial profiles of the simulated data in the axial regions of 110-160 mm and 240-290 mm. The electron density is peaked at the vessel center and reaches its axial value of $2 \cdot 10^{17}$ m^{-3}. It can be well described by the plotted Bessel profile, which is typically found in cylindrically symmetric discharges [22]. The electron energy depicts an inverse profile, with its minimum of 9 eV on the cylinder axis increasing up to almost 11 eV near the actual RF heating region at the vessel boundary.

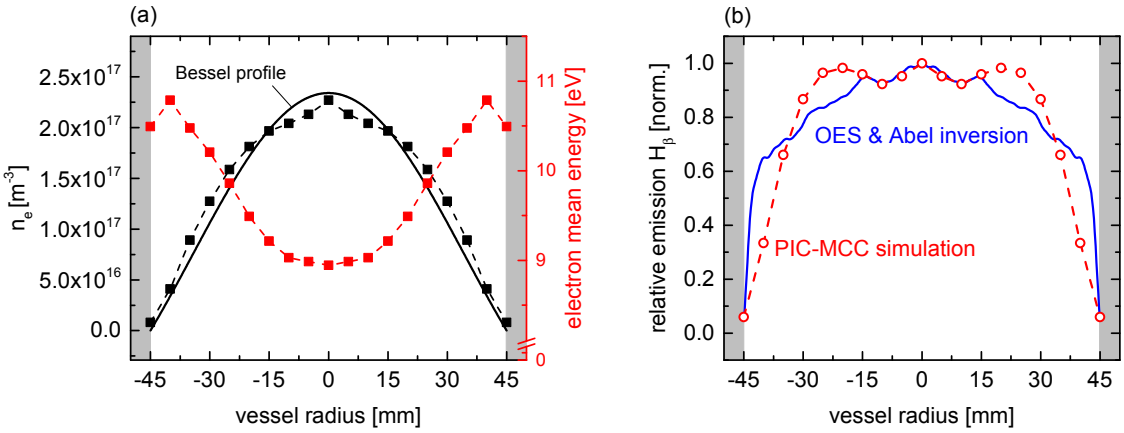

FIGURE 4. (a) Radial profile of the electron energy and density provided by the PIC-MCC model at a pressure of 1 Pa, including a Bessel profile fit of n_e (b) Comparison of the normalized emission profile of the atomic H_β emission line measured via OES and the emission evaluated by calculation the rate of electron collision excitation of the $n = 4$ atomic state based on the plasma parameters shown in (a).

The validity of the presented profiles is examined by a comparison with the measured radial emission profiles of the atomic H_β emission line ($n = 4 \rightarrow n = 2$). Based on the simulated profiles $n_e(r)$ and $E_e(r)$, the radially resolved emission due to electron collisional excitation of the upper state $n = 4$ is calculated. Assuming a constant ground state density and a Maxwellian EEDF, the emissivity $\epsilon(r)$ is proportional to the product $n_e(r) \cdot X(T_e(r))$. The rate coefficient $X(T_e)$ is calculated based on cross section data provided by [23]. The normalized emission profile gained by this approach is presented in Figure 4 (b), compared to the emission profile evaluated via OES and Abel inversion which was measured at a corresponding axial position. For both methods, a steep increase of the emission at the cylinder walls followed by a relatively broad maximum in the vessel centre is observed. Generally, a good agreement between the profiles can be found. The conspicuously detailed correspondence of both profiles near the centre has to be considered incidental, as such small variations are within the statistical errors of both methods. Deviations are present particularly near the cylinder walls, as the slope of the simulated profile remains basically constant until the maximum is reached, whereas the measured profile almost immediately jumps to 60 % of the maximum emission and then gradually increases. However, especially in this region the uncertainties of both the simulation (due to the relatively large spatial resolution of 5 mm cell size) as well as the OES measurements (due to a very short LOS and possible reflections within the quartz vessel) are high. Nevertheless, the general agreement in combination with the results of the axial comparison indicate, that also the basic radial behaviour of the plasma parameters is indeed well represented by the modelled profiles.

CONCLUSION

The RF power required at negative hydrogen ion sources for fusion is substantial. As this poses strong demands on the generators and all components of the RF circuit, an reduction of the power would be highly desirable. Fundamental investigations regarding the RF coupling efficiency in hydrogen and deuterium are performed at the lab experiment CHARLIE. The presented investigations have been performed in hydrogen for the RF power of 520 W delivered by the 1 MHz generator at varying pressure utilizing a helical ICP coil for plasma generation. The evaluated RF coupling efficiency is peaked at 85 % for pressures between 1 and 3 Pa and decreases particularly at low pressures. At 0.3 Pa, the relevant operating pressure of ion sources for fusion, only 50 % of the delivered power contribute to plasma heating. However, this is only valid for this specific scenario, as the RF coupling typically increases for higher powers also at low pressures. The measured electron density, which is of the order of 10^{17} m^{-3}, is well correlated with the pressure dependent behaviour of the coupling efficiency.

In order to gain additional spatially resolved insight of the RF heating mechanism, first simulations of the discharge are conducted by an electromagnetic PIC-MCC method, providing spatial distributions of the electron density

and mean energy based on the real experiment geometry, the measured antenna current and the prevailing neutral particle density. The comparison of the simulated data with both axially resolved probe measurements and radially resolved emission profiles at 1 Pa shows a good general agreement, revealing the radial distribution of the electron density to be well described by a Bessel profile.

ACKNOWLEDGMENTS

This work has been carried out within the framework of the EUROfusion Consortium and has received funding from the Euratom research and training programme 2014-2018 under grant agreement No 633053. The views and opinions expressed herein do not necessarily reflect those of the European Commission.

REFERENCES

[1] R. Hemsworth et al., Nuclear Fusion **49**, p. 045006 (2009).
[2] D. Marcuzzi et al., Fusion Engineering and Design **82**, 798 – 805 (2007).
[3] D. Wünderlich et al., Plasma Sources Science and Technology **23** (2014).
[4] J. Hopwood, Plasma Sources Sci. Technol. **3**, 460–464 (1994).
[5] E. A. Kral'kina, Physics-Uspekhi **51**, 493–512 (2008).
[6] V. A. Godyak and R. B. Piejak, Journal of Vacuum Science & Technology A **8**, 3833–3837 (1990).
[7] S. Briefi et al., Plasma Sources Science and Technology **25**, p. 035015 (2016).
[8] S. Briefi, P. Gutmann and U. Fantz, AIP Conference Proceedings **1655** (2015).
[9] D. Rauner et al., Proc. of 32nd ICPIG (Iasi) (2015).
[10] S. Mattei et al., Contribution to these Proceedings (2016).
[11] E. O. Johnson and L. Malter, Phys. Rev. **80**, 58–68 (1950).
[12] F. F. Chen, J. D. Evans and W. Zawalski, in *Plasma Diagnostic Techniques* (Academic Press, 1965), pp. 113–199.
[13] U. Fantz, Contributions to Plasma Physics **44**, 508–515 (2004).
[14] S. Briefi et al., to be published .
[15] D. Wünderlich et al., JQRST **110**, 62–71 (2009).
[16] D. Wünderlich et al., Proc. of the 30th ICPIG, Belfast (2011).
[17] R. Alvarez, A. Rodero and M.C. Quintero, Spectrochimica Acta Part B: Atomic Spectroscopy **57**, 1665 – 1680 (2002).
[18] E. A. Kralkina et al., Plasma Sources Science and Technology **25**, p. 015016 (2016).
[19] P. Chabert and N. Braithwaite, *Physics of Radio-Frequency Plasmas* (Cambridge, 2011).
[20] H. Tawara et al., Journal of Physical and Chemical Reference Data **19**, 617–636 (1990).
[21] V.A. Godyak, R.B. Piejak and B.M. Alexandrovich, Plasma Sources Science and Technology **1**, 36–58 (1992).
[22] L. Tonks and I. Langmuir, Phys. Rev. **34**, 876–922 (1929).
[23] R.K. Janev, D. Reiter and U.Samm, Forschungszentrum Jülich, Report Jül–4105 (2003).